# Documenting evapotranspiration and surface energy fluxes over rainfed annual crops within a Mediterranean hilly agrosystem

Rim Zitouna-Chebbi [a,*], Frédéric Jacob [b], Laurent Prévot [b], Marc Voltz [b]

[a] Carthage University, National Research Institute in Rural Engineering, Waters and Forests, LR16INRGREF02 - LRVENC, Ariana, Tunisia
[b] LISAH, University of Montpellier, AgroParisTech, INRAE, Institut Agro Montpellier, IRD, Montpellier, France

ABSTRACT

The current study aims to document evapotranspiration and associated surface energy fluxes for rainfed annual crops within a Mediterranean hilly agrosystem, in order to provide information on crop water use under such little-studied conditions. For this, an experimental study is conducted within the Tunisian study site of the OMERE observatory (French acronym for the Mediterranean Observatory of Water and the Rural Environment), located in the north-eastern Cap Bon peninsula. It relies on eddy covariance (EC) measurements at the plot scale. We report that (1) observations are consistent with previous studies under Mediterranean or semi-arid contexts, with time series of energy fluxes that depict classical seasonal dynamics, (2) common flux ratios (i.e., Bowen Ratio, ratio of actual to reference evapotranspiration) may change according to upwinds and downwinds, which requires further investigations about possible changes in aerodynamic conditions, and (3) a reference evapotranspiration value of 4 mm day$^{-1}$ seems to be a threshold beyond which actual evapotranspiration decreases systematically and rapidly. In terms of agricultural water management, the current study suggests to look for early sowing species/varieties, in order to reduce the evaporation-based water loss in autumn. Overall, EC measurements seem promising over rainfed annual crops within semiarid hilly agrosystems, for long term observations, environmental modelling and operational purposes. Since the current study is conducted over few small fields within a specific hilly topography, the original results we report here need to be strengthened with complementary studies.

## 1. Introduction

The southern shore of the Mediterranean region has limited water resources. Water scarcity is likely to increase under climate change impact, with consequences on crop functioning and yields (Brouziyne et al., 2018; Vadez et al., 2022). The combination of crop yield decrease and population growth is likely to induce food insecurity and rural exodus (Weiss et al., 2020; Zouabi, 2021). Such forecast is critical for rainfed annual crops, where plants with shallow rooting systems do not benefit from irrigation (Hossain et al., 2020). In this context, there are pressing demands for optimising crop water consumption by means of different techniques such as changes in crop variety or on-farm practices (Karrou and Oweis, 2012).

The optimisation of crop water consumption within agrosystems can be explored using numerical tools that address crop functioning and hydrological cycle, including modelling platforms (Lebon et al., 2019; Siad et al., 2019) and learning machine methods (Cheng et al., 2022;

Elbeltagi et al., 2020), where both approaches rely on long-term observations (Jarlan et al., 2015; Molénat et al., 2018). Within Mediterranean rainfed agrosystems, annual crops functioning is mainly driven by root zone water content, while evapotranspiration is the most significant term of the hydrological balance (Aouade et al., 2020). Thus, several numerical tools rely on first order relations between plant transpiration and biomass production (Dhouib et al., 2022; Ran et al., 2020), while their calibrations require complementary observations of plant growth, root zone water content and evapotranspiration (Kanda et al., 2021; Yang et al., 2019).

Hilly catchments are widespread around the Mediterranean. Their topography allows for water harvesting techniques that compensate for rainfall shortage by increasing infiltration, such as land use or hydro-agricultural structures (Ammar et al., 2016; Harmanny and Malek, 2019; Mekki et al., 2006). Thus, margin progresses are explored within hilly rainfed agrosystems, by modulating changes in cropping systems and water harvesting techniques (Al-Khuzaie et al., 2020; Grum et al.,

2017). When dealing with water consumption, it is necessary to account for additional processes induced by topography, for both observation and modelling. This includes (1) changes in solar radiation with slope orientation (Nie et al., 1992), (2) changes in soil depth, soil moisture and vegetation growth along upstream-downstream transects (Tromp-van Meerveld and McDonnell, 2006), and (3) changes in air streamlines within the boundary layer, in aerodynamic and micrometeorological conditions, in source contributions, and consequently in convective fluxes (Chen et al., 2019; Finnigan et al., 2015).

Several studies have addressed micrometeorology and boundary layer turbulence over sloping and heterogeneous terrains, mainly for mountainous conditions (Hammerle et al., 2007; Hiller et al., 2008; Serrano-Ortiz et al., 2016). However, very few studies dealt with crop water consumption for rainfed annual crops within Mediterranean hilly catchments, whereas the latter differ from mountainous conditions because of (1) the absence of anabatic and katabatic winds, (2) the absence of valley breeze along catchment longitudinal axis, and (3) the presence of externally driven winds that induce forced convection with neutral conditions (Zitouna-Chebbi et al., 2015, 2012). When dealing with modelling, few works focused on the performances of crop models designed for flat terrains (Boudhina et al., 2019), the formulation of aerodynamic resistance (Rana et al., 2007), and the tailoring of variables within the Penman-Monteith equation (Rana et al., 2011). When dealing with observation, few studies investigated (1) the processing of eddy covariance (EC) measurements according to upwinds/downwinds and to vegetation height (Zitouna-Chebbi et al., 2015, 2012), (2) the assessment of EC measurements according to sloping conditions (Boudhina et al., 2017, 2018a), and (3) the tailoring of gap filling methods according to upwinds and downwinds (Boudhina et al., 2018b; Zitouna-Chebbi et al., 2018).

Beyond the aforementioned works on data processing and gap-filling, obtaining times series of crop water consumption over several crop cycles is paramount. It permits to study the temporal dynamics of root zone soil water content, crop functioning and water consumption (Longobardi and Villani, 2013). It opens path to documenting water fluxes over large periods, in relation to hydrological cycle and crop water consumption (French et al., 2020; Liu et al., 2012; Payero and Irmak, 2013; Talebizadeh et al., 2018). It permits to document long-term influence of anthropogenic and climate forcing (Molénat et al., 2018). Several efforts have been conducted to produce and analyse times series of evapotranspiration over vegetated land surfaces, including irrigated maize (Dare-Idowu et al., 2021), irrigated wheat (French et al., 2020; Rafi et al., 2019), irrigated cotton (Anapalli et al., 2020), and rainfed chickpea (Chakraborty et al., 2021). However, and to our best knowledge, no study addressed rainfed annual crops within Mediterranean hilly agrosystems, whereas specific trends are likely to be observed in such context, because of differences in soil depth, soil moisture within shallow rooting systems, vegetation growth, and insolation / aerodynamic conditions that drive convective fluxes.

The main objective of the current study is to document evapotranspiration and related surface energy fluxes over rainfed annual crops within a Mediterranean hilly agrosystem. This main objective is broken down into two specific objectives, in relation to existing knowledge. A first specific objective is to account for upwinds and downwinds, follow on from the aforementioned studies that reported the influence of such winds on data processing and gap filling. A second specific objective is to analyse evapotranspiration and surface energy fluxes, as well as several proxies that document on vegetation water status. For this, we analyse fluxes and related ratios by considering daily timescale and annual extent, in relation to crop phenology and hydrometeorological conditions. To reach the main objective and specific objectives, we conduct an experimental study within a hilly agrosystem located in the Cap Bon peninsula, north-eastern Tunisia, over four rainfed annual crops that are representative of the Mediterranean context.

The current paper is structured as follows. We first detail the materials, including the experimental setup and the measurement features, the experimental conditions, the data processing, and the strategy for producing complete time series of energy fluxes. Thereafter, we simultaneously report and discuss the results we obtain for energy fluxes and related ratios, when considering the daily timescale and the annual extent. We finally conclude on the contribution of the current study to the knowledge of evapotranspiration for rainfed annual crops within Mediterranean hilly agrosystems, along with further perspectives.

## 2. Materials and methods

### 2.1. Study area: the Kamech catchment

The experiment takes place within the Kamech experimental site (2.5 km$^2$), which is a sub-catchment of the Lebna regional catchment (210 km$^2$) located in the Cap Bon Peninsula, north-eastern Tunisia (36°52′40″ N, 10°52′40″ E, 108 m above sea level). Kamech belongs to the long-term environmental research observatory OMERE (French acronym for the Mediterranean Observatory of Water and the Rural Environment). A detailed description of Kamech is given in Mekki et al. (2006), and a detailed description of the OMERE observatory is given in Molénat et al. (2018).

The catchment topography is V-shaped along the northeast-southwest axis. The altitude ranges from 94 m to 194 m, the terrain slope ranges from 0 % to 30 %. The soil depth ranges from a few millimetres to two metres, according to the location within the catchment and to the local topography. The catchment includes four dominant soil types (Mekki et al., 2018), namely Cambisols (46 % of the catchment area), Luvisols (26 %), Vertisols (10 %) and Regosols (18 %). The soils have sandy-loam textures, which make them swelling soils that exhibit shrinkage cracks under dry conditions during the summer (Raclot and Albergel, 2006). The regional climate is at the frontier between sub-humid and semi-arid, with annual values of 667 mm and 1336 mm for rainfall and Penman-Monteith evapotranspiration, respectively (average values over the [2004–2006] period).

The main crops are rainfed, including winter cereals (durum and bread wheat, barley, oat, triticale) and legumes (chickpeas, faba bean). These crops can be harvested or grazed. The steepest parts of the catchment are covered by natural vegetation, and used as rangelands for grazing. Agricultural land parcel is typified by small plots with an average size of 0.62 ha. A small hilly dam is set at the outlet of the Kamech sub-catchment, and belongs to the network of small hilly dams along the hydrographic network within the regional Lebna catchment (Gaubi et al., 2017).

### 2.2. Measurement location and calendar

In line with the previous works aforementioned, we rely in the current study on the use of eddy covariance (EC) systems for measuring convective fluxes (i.e., sensible and latent heat fluxes), along with classical measurement devices for net radiation and soil heat flux. In relation to the footprint of the EC measurements, which can extend over several tens of metres depending upon airflows within the boundary layer (Aubinet et al., 2012), we select agricultural plots larger than 1 ha, so that any EC footprint mainly extends within the corresponding plot. Additionally, we select (1) plots with regular slope to avoid transient airflows within the EC footprint, and (2) plots far from the outlet dam to avoid possible advection. These constraints lead to select three plots labelled A, B and C (Fig. 1).

Field data are collected throughout vegetation growth cycles in plots A, B and C. The experiment is conducted in 2004, 2005 and 2006, and it encompasses successions of vegetation growth and bare soil after harvest or grazing. The corresponding four datasets are labelled A04, B05, A06 and C06, where the letter represents the plot, and the two digits represent the year. Detailed descriptions of both topography and relative position within the catchment for these plots are given in, Zitouna-Chebbi et al. (2015, 2012). We briefly synthesise here the area, the
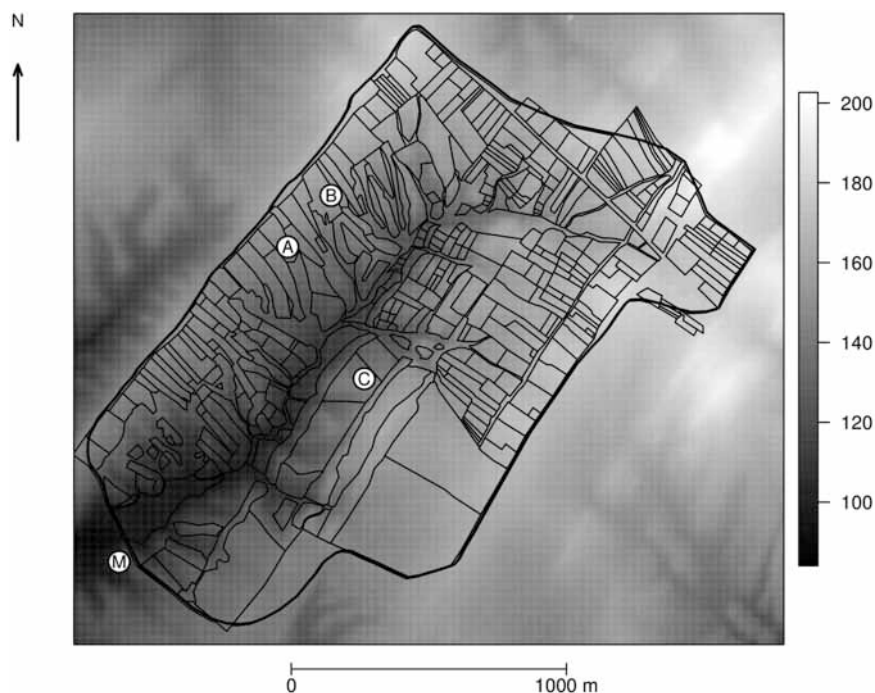
**Fig. 1.** Topography of the Kamech catchment deduced from a 4-m spatial resolution digital elevation model (DEM). Altitude above sea level is given in metres (right greyscale bar). The thick black line represents the catchment outline, and the thin black lines represent the plot limits. The position of the agro-meteorological station (M) and of the flux stations on plots A, B and C are represented by the white circles.

slope, the soil type, the period of experiment and the land use (Table 1).

### 2.3. Data collection: agro-meteorological data, energy flux data, vegetation data

A agro-meteorological station is located near the catchment outlet (labelled M), to perform the following measurements: (1) rainfall at a daily time step with a manual rain gauge (ORE OMERE HYSAE database, https://www.umr-lisah.fr/hysae/); (2) solar irradiance with a SP1110 pyranometer (Skye, UK); (3) air temperature and humidity with an HMP45C probe (Vaisala, Finland); (4) wind speed with an A100R anemometer (Vector Instruments, UK); and (5) wind direction with a W200P wind vane (Vector Instruments, UK). The instruments are installed 2 m above ground (except the rain gauge, which is installed 1 m above ground level), and they are connected to a CR10X data-logger (Campbell Scientific, USA). Apart from rainfall, variables are sampled at a 1 Hz frequency, averaged and stored with a 30-mn time step. All instruments are new or recently new, and are calibrated by the manufacturer.

One or two eddy covariance (EC) stations are installed on different plots in 2004, 2005 and 2006, to measure sensible and latent heat fluxes at the plot scale (Fig. 1 and Table 1). In 2004 (respectively 2005) an EC station is installed on plot A (respectively plot B). In 2006, an EC station

is installed on both plot A and C.

- Each EC station measures wind speed in three dimensions (u and v are horizontal coordinates, w is vertical coordinate) and air temperature (T) with a CSAT3 sonic anemometer (Campbell scientific, USA) for datasets A04, B05, A06 and with a Young-81000V sonic anemometer (R.M. Young, USA) for dataset C06. Each EC station also measures specific humidity (q) with a KH20 krypton hygrometer (Campbell scientific, USA) for datasets A04 and C06 (the KH20 does not operate for datasets A06 and B05 because of instrumental degradation). The raw data of the sonic anemometer and of the krypton hygrometer are recorded with a 10 Hz frequency, they are stored in a CR23X datalogger (Campbell Scientific, USA), and they are downloaded every minute to a laptop through a RS232 serial port. Additionally, the CR23X datalogger directly calculates convective fluxes without any prior instrumental correction. The goal is to produce complete time series of evapotranspiration thanks to gap filling approaches. The process is briefly explained in Section 2.6 and detailed in Supplementary materials - Section 1.
- A HMP45C probe (Vaisala, Finland) is installed on each EC station to measure air temperature and humidity and next correct the calibration drift of the krypton hygrometer. Net radiation (Rn) is measured at each EC station using a NR-lite device (Kipp & Zonen,

**Table 1**
Presentation of the four datasets A04, B05, A06 and C06, including the plot, the area, the slope, the soil texture and depth, the period of experiment and the land use.

| Dataset | Year | Plot | Area (ha) | Slope | Soil texture and depth | Period of experiment | Land use |
|---|---|---|---|---|---|---|---|
| **A04** | 2004 | A | 1.1 | 5° facing south-southeast | Sandy clay loam < 1.5 m | March 30–November 4 | Wheat Bare soil |
| **A06** | 2006 | | | | | March 3–July 28 | Faba bean Rangeland Bare soil |
| **B05** | 2005 | B | 1.6 | 5° facing south-southeast | Clay loam > 1.5 m | January 18–June 20 | Oat Bare soil |
| **C06** | 2006 | C | 2.2 | 8° facing northwest | Silty clay < 1 m | April 13–July 27 | Rangeland Bare soil |

NL). The net radiometers are installed 1.5 m above the ground. Soil heat flux (G) is measured at each EC station using three HFP01 soil heat flux plates (Hukseflux, Netherlands) that are distributed two metres away from the station, and are buried between 2 and 5 cm below the soil surface. These measurements are recorded with a 1 Hz frequency, they are next averaged and stored with a 30-mn time step in the CR23X datalogger.

- The sonic anemometers, the krypton hygrometers, and the air temperature and humidity probes are installed at the same height above the ground during each period of data acquisition: 1.96 m for Field A in 2004 (data set A04); 1.78 m for Field A in 2006 (dataset A06); and 2.02 m for Field C in 2006 (data set C06). Zitouna-Chebbi et al. (2015, 2012) verified that (1) 70–80 % of each flux measurement originated from the corresponding field with a unique crop, and (2) the measurement heights were located within the inertial sublayer above the roughness sublayer regardless of vegetation height.

Vegetation measurements include plant height and leaf area index (LAI). For plant height, the number of observations per plot ranges from 30 for annual crops (homogeneous canopies) to 100 for rangelands (heterogeneous canopies with several species), for each measurement date. For LAI, sample collection is replicated within delimited areas of $0.30 \times 0.30$ m$^2$ size, at each measurement date. The number of replicates per plot varies from 5 to 10 depending upon the canopy heterogeneity. For both plant height and LAI, frequency of measurement collection ranges from 2 to 4 weeks, in accordance to the vegetation growth observed within each plot. Plant height is estimated using a tape measure, and each sample is weighed. Next, a sub-sample is selected, corresponding to about 1/3 of the sample weight, to measure leaf area using a WinDIAS planimeter (DELTA-T Devices Ltd, Cambridge, UK). Finally, plant height and leaf area index at the plot scale are estimated as average values across all samples, for each date.

### 2.4. Characterisation of experimental conditions

#### 2.4.1. Vegetation conditions

For each dataset, we provide an overview about crops and varieties, as well as about vegetation development throughout growth cycle. Following Allen et al. (1998), we using leaf area index LAI and vegetation height. Table 2 summarises vegetation growth stage, as well as measurements of LAI and plant height throughout the experiment.

The experiment starts on plot A in 2004 (dataset A04) when durum wheat crop (Karim variety, common in North Africa) is at full development stage (FD). Agricultural practices are not optimal, and we note the presence of both weeds and diseases (wheat rust). LAI reaches his maximum value (LAI_max) at the end of March, with a value of 0.8 m$^2$ m$^{-2}$. The senescence stage (SE) starts on 26 May. After harvest on 17 July, the plot is used for grazing, and it is covered by wheat straw residues that slowly decompose until the end of the summer. The first ploughing for next crop is done at the beginning of November 2004.

The experiment starts on plot B in 2005 (dataset B05) one month after sowing, when oat (local variety) is at mid-season development stage (MD). The FD stage starts on 01 April, with an LAI_max equal to 3 m$^2$ m$^{-2}$ on average and a plant height equal to 1 m on average. Senescence stage (SE) starts on 25 May, and the oat crop is green cut at the end of May for animal feeding.

The experiment starts on plot A in 2006 (dataset A06) with a faba bean crop "Vicia faba L." (local variety). Measurements start during the MD stage, and the FD stage occurs on 28 March (LAI_max = 1.34 m$^2$ m$^{-2}$, plant height = 0.45 m). After harvest of the pods in mid-May, the plot is used for grazing with natural vegetation until the dry period.

During 2006, another experiment is conducted on plot C (dataset C06). Plot C is not cultivated and spontaneous vegetation is used for grazing. Vegetation canopy is very heterogeneous. The measurements start at FD stage with LAI_max = 0.92 m$^2$ m$^{-2}$, and SE stage starts on 18 May. The spontaneous vegetation depicts a similar dynamic than cultivated crops, with similar periods of greenness and senescence.

**Table 2**

Vegetation growth stages, along with measured LAI and plant height (average values at the plot scale) for the four datasets A04, B05, A06 and C06 that correspond to durum wheat, oat, faba bean and rangeland, respectively. MD, FD, SE and H stand for mid-season development stage, full development stage, senescence and harvest, respectively.

**A04: Durum Wheat (Karim variety)**

| | | | | | |
|---|---|---|---|---|---|
| Date in 2004 | 30/03 | 07/04 | 05/05 | 26/05 | 17/07 |
| Day of the year | 90 | 98 | 126 | 147 | 199 |
| Growth stage | FD | FD | FD | SE | Harvest |
| LAI (m$^2$ m$^{-2}$) | 0.8 | 0.3 | 0.8 | 0.3 | |
| Height (m) | 0.56 | 0.68 | 0.61 | 0.65 | 0.65 |

**B05: Oat (local variety)**

| | | | | | | | | | |
|---|---|---|---|---|---|---|---|---|---|
| Date in 2005 | 07/02 | 23/02 | 23/03 | 01/04 | 15/04 | 20/04 | 25/04 | 05/05 | 24/05 |
| Day of the year | 38 | 54 | 82 | 91 | 105 | 110 | 115 | 125 | 144 |
| Growth stage | MD | MD | MD | FD | FD | FD | FD | SE | H |
| LAI (m$^2$ m$^{-2}$) | 1.1 ± 0.4 | | 1.5 ± 0.6 | 2.9 ± 1.2 | | 2.8 ± 1.2 | 3 ± 1 | | |
| Height (m) | | 0.18 | 0.38 | 0.51 | 0.6 | | | | 0.95 |

**A06: Faba bean (local variety)**

| | | | | | |
|---|---|---|---|---|---|
| Date in 2006 | 04/03 | 28/03 | 20/04 | 18/05 | 31/05 |
| Day of the year | 63 | 87 | 110 | 138 | 151 |
| Growth stage | MD | FD | FD | H weeds | weeds |
| LAI (m$^2$ m$^{-2}$) | 0.8 ± 0.23 | 1.34 ± 0.79 | 0.52 ± 0.28 | 0.57 ± 0.22 | 0.46 ± 0.20 |
| Height (m) | 0.3 | 0.43 | 0.45 | 0.33 | 0.33 |

**C06: Rangeland mixture of natural vegetation**

| | | |
|---|---|---|
| Date in 2006 | 04/05 | 18/05 |
| Day of the year | 124 | 151 |
| Growth stage | FD | SE |
| LAI (m$^2$ m$^{-2}$) | 0.92 | 0.56 |
| Height (m) | 0.4 | 0.51 |

### 2.4.2. Meteorological conditions

We characterise climatic conditions during the experiment on the basis of daytime values of air temperature (Ta), solar radiation (Rg), wind speed (U) and vapour pressure deficit (VPD), where daytime corresponds to solar and net radiation above 20 W m$^{-2}$. These meteorological variables are collected by the agro-meteorological station located at the outlet of the Kamech catchment (Section 2.3).

A prerequisite for the analysis of these variables is to obtain complete time series throughout the experiment, despite missing data due to equipment malfunction, mainly for measurements of air temperature and humidity. To this end, we use linear relationships between half-hourly values of air temperature and humidity from coincident measurements with HMP45C probes at the agro-meteorological station and the EC stations. These linear relationships are typified by (1) correlation coefficients R$^2$ around 0.99, and (2) discrepancies around the regression lines around 0.1 °C and 0.03 kPa for air temperature and VPD, respectively. Next, daily reference evapotranspiration (ET$_0$) is calculated using FAO56 method according to Allen et al. (1998).

Table 3 displays daytime values when separating winds from the northwest sector (wind direction greater than 220 and less than 70°), and winds from the south sector (wind direction between 135° and 225°), as well as when separating conditions of vegetated surface and bare soil.

- Rg ranges from 384 W m$^{-2}$ for dataset A04 with bare soil to 560 W m$^{-2}$ for dataset C06 with bare soil. On plot A in 2004, Rg is low during the bare soil period in autumn. Neither systematic nor significant difference is observed between northwest and south winds.
- U ranges from 4 and 6.4 m s$^{-1}$, which corresponds to large values as compared to FAO worldwide mean value (Allen et al., 1998). These large wind speed values are in agreement with the micrometeorological data that indicated dominant regimes of forced convection along with conditions of near-neutrality or low instability (Zitouna-Chebbi et al., 2012). South winds are typified by lower speeds as compared to northwest winds.
- Ta ranges from 13 to 30 °C, which is representative of the seasonal variability throughout the experiment. We note larger Ta values for south winds as compared to northwest winds, with differences ranging from 1 to 3 °C.

**Table 3**

Mean daily climatic data for solar radiation (Rg), wind speed (U), air temperature (Ta) and vapour pressure deficit (VPD), for each of the four datasets A04, B05, A06 and C06. We separate northwest winds and south winds, and we separate vegetated surfaces and bare soils. Mean daily climatic data correspond to daytime values.

| | Rg (W m$^{-2}$) | | U (m s$^{-1}$) | | Ta (°C) | | VPD (kPa) | |
|---|---|---|---|---|---|---|---|---|
| | NW | S | NW | S | NW | S | NW | S |
| A04 wheat 30/03–17/07 | 491 | 518 | 5.1 | 4.2 | 20.0 | 21.8 | 0.89 | 1.22 |
| A04 bare soil 18/07–04/11 | 384 | 387 | 5.3 | 4.4 | 21.7 | 24.4 | 1.02 | 1.30 |
| B05 oat 18/01–24/05 | 398 | 484 | 6.4 | 4.3 | 13.5 | 17.0 | 0.49 | 0.72 |
| B05 bare soil 25/05–20/06 | 530 | 486 | 5.0 | 3.8 | 23.0 | 24.5 | 0.11 | 1.39 |
| A06 faba bean 03/03–16/05 | 470 | 488 | 6 | 4.3 | 15.6 | 17.8 | 0.65 | 0.68 |
| A06 rangeland 17/05–20/06 | 512 | 549 | 5.2 | 4.6 | 21.2 | 25.2 | 1.20 | 1.70 |
| A06 bare soil 21/06–28/07 | 559 | 514 | 4.6 | 4.0 | 27.0 | 30.1 | 1.50 | 2.80 |
| C06 rangeland 13/04–20/06 | 508 | 533 | 5.1 | 4.3 | 19.8 | 22.2 | 1.02 | 1.23 |
| C06 bare soil 21/06–27/07 | 560 | 513 | 4.6 | 4.0 | 27.1 | 30.7 | 1.59 | 2.82 |

- VPD varies between 0.11 kPa for bare soil conditions on plot A in 2004, and 2.8 kPa for bare soil conditions on both plot A in 2006 and plot C in 2006. South winds are typified by larger VPD values as compared to northwest winds, since they correspond to larger air temperatures values.

Fig. 2 displays times series of daily rainfall for 2004, 2005 and 2006. Yearly cumulated rainfall (R) is 515 mm, 726 mm and 761 mm, respectively. Daily rainfall depicts an inter-seasonal variability. Cumulated rainfall is larger for northwest winds as compared to south winds, which results from the combination of (1) similar average values for both with directions and (2) a larger occurrence of northwest winds. From a seasonal viewpoint that combines rainfall with vegetation growth stage, larger cumulated rainfalls are recorded during the mid-development (MD) stage than during the full-development (FD) stage, for datasets B05, A06 and C06.

Fig. 2 also displays times series of daily reference ET$_0$. Cumulated values at the yearly timescale are 1427 mm, 1252 mm and 1329 mm for 2004, 2005 and 2006 respectively. Daily ET$_0$ ranges from 1 to 8 mm day$^{-1}$, and largest values are observed when maximum values occur for both air temperature and VDP. Thus, the winter season (respectively summer season) corresponds to lowest values (respectively largest values) of ET$_0$. During the summer season, ET$_0$ is larger for south winds as compared to northwest winds, whereas it is similar regardless of wind direction during the other seasons.

When comparing rainfall against ET$_0$ for different stages of vegetation development, we observe that daily rainfall (R) is larger than daily ET$_0$ only for the B05 dataset during the mid-development (MD) stage, with R = 3.56 mm day$^{-1}$ and ET$_0$ = 1.93 mm day$^{-1}$ on average over the period. Daily water supply is heterogeneously distributed throughout the vegetation growth cycle. Overall, the meteorological conditions of the Kamech catchment are typically Mediterranean, with a water limitation during the summer and an energy limitation during the winter.

### 2.5. Flux data processing

Half-hourly data of net radiation (Rn) are corrected from sloping effect on solar exposure by following (Holst et al., 2005), as detailed in Zitouna-Chebbi et al. (2012). In addition, a side-by-side comparison of NR-lite net radiometers is conducted during one month within the same plot. Instrumental differences are within the instrumental accuracies, with a root mean square difference (RMSD) of about 20 W m$^{-2}$. The three soil heat flux measurements (G) are averaged over 30-mn periods, and no correction is applied for the heat storage between the surface and the sensors. We chose not to apply any correction since existing corrections are questionable for swelling soils (Zitouna-Chebbi et al., 2015, 2012).

As mentioned previously, the CR23X datalogger also calculates convective fluxes without any prior instrumental correction, in order to produce complete time series of evapotranspiration. Convective fluxes are calculated as H = ρ.Cp.cov(w,T) for sensible heat, and LE = ρ.Lv.cov(w,q) for latent heat, where ρ is air density, Cp is air specific heat, Lv is vaporisation latent heat, w and t are vertical wind speed and air temperature measured by the sonic anemometer, q is specific humidity measured by the krypton hygrometer, and cov stands for covariance. Sensible and latent heat fluxes are calculated over 30-mn periods and stored in the CR23X datalogger. They are labelled H_WC for sensible heat and LE_WC for latent heat, where WC stands for without correction.

The raw data recorded at 10 Hz are postprocessed using the ECPACK open-source library - version 2.5.22 (Van Dijk et al., 2004). Postprocessing steps include spike detection (Vickers and Mahrt, 1997), air humidity corrections for sensible heat flux (Schotanus et al., 1983), density corrections for latent heat flux (Webb et al., 1980) and planar fit rotation (Wilczak et al., 2001). When applying planar fit rotation, we account for the influence of hilly topography by separating upwinds and downwinds, and by separating different intervals of vegetation height
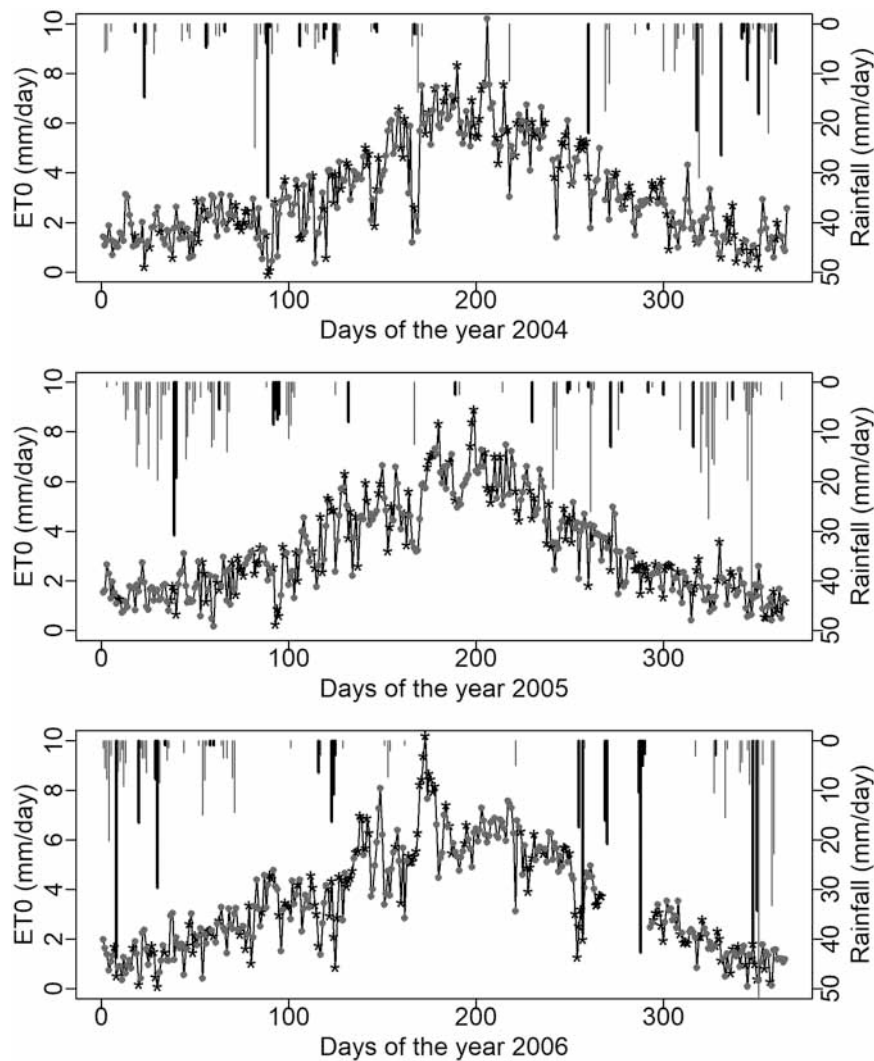
**Fig. 2.** Daily rainfall (mm day$^{-1}$) and reference evapotranspiration ET$_0$ (mm day$^{-1}$) for the three years of experiment, namely 2004, 2005 and 2006. Daily ET$_0$ corresponding to south and northwest winds are indicated by black and grey colour respectively.

(Zitouna-Chebbi et al., 2015, 2012). Convective fluxes are calculated over 30-mn periods. Next, we apply quality control tests to select EC high-quality data (Foken and Wichura, 1996). For this, we keep the two first classes of quality control test, since they are considered as high quality data for long term flux estimation (Foken et al., 2005). These convective fluxes are labelled H_PF for sensible heat and LE_PF for latent heat, where PF stands for planar fit.

Eventually, each dataset (A04, A06, B05 and C06) includes a number of 30-mn data for each energy flux and each processing level on convective fluxes. The number of data depends upon the length of data acquisition period, the daytime length throughout the data acquisition period, the data availability, and the quality filtering. Table 4 indicates the numbers of data for Rn and G, for H_WC and LE_WC, as well as for H_PF and LE_PF. When dealing with Rn, datasets cover all measurement periods. As compared to the number of Rn data within each dataset, we note slight missing rates for G within datasets A04 and B05, about 0.1 % and 3.8 %, respectively. For H_WC and LE_WC, we note moderate missing rates when measurements are available, from 12.5 % to 34.8 % and from 33.4 % to 44.6 %, respectively. For H_PF and LE_PF, we note significant missing rates when measurements are available, from 58.4 % to 89.8 % and from 63.2 % to 91.8 %, respectively. These significant missing rates stem from experimental troubles for data storage in relation to power failure. For convective fluxes with correction H_PF and LE_PF, the few numbers of data highlight the necessity to use gap filling

**Table 4**

Number of 30-mn flux data for the four datasets (A04, B05, A06, C06), including net radiation (Rn) and soil heat flux (G), sensible heat and latent heat flux without correction (H_WC and LE_WC), as well as sensible heat and latent heat flux after instrumental corrections, planar fit correction and control quality filtering (H_PF and LE_PF). PED stands for percentage of existing data according to the number of net radiation data.

| Dataset | Rn | G (PED %) | H_WC (PED %) | LE_WC (PED %) | H_PF (PED %) | LE_PF (PED %) |
|---------|------|-----------|--------------|---------------|--------------|---------------|
| **A04** | 4293 | 4288 (99.9) | 3758 (87.5) | 2860 (66.6) | 438 (10.2) | 351 (8.2) |
| **B05** | 3113 | 2994 (96.2) | 2468 (79.3) | – | 826 (26.5) | – |
| **A06** | 3163 | 3163 (100.0) | 2437 (77.0) | – | 1167 (36.9) | – |
| **C06** | 2267 | 2267 (100.0) | 1479 (65.2) | 1256 (55.4) | 943 (41.6) | 834 (36.8) |

methods, based on available data of net radiation and of convective fluxes without correction H_WC and LE_WC.

*2.6. Generating time series of convective fluxes*

Table 4 in Section 2.5 highlights the low percentages of data

available for convective fluxes, relative to the numbers of data to be collected throughout the experiment duration, as indicated with the number of available data for net radiation. In order to document evapotranspiration and surface energy fluxes under the specific conditions on which focuses the current study, namely rainfed annual crops within a Mediterranean hilly agrosystem, we set up and implement an overall strategy to produce times series of convective fluxes, for each of the datasets A04, B05, A06 and C06.

We produce time series of surface energy fluxes at the half-hourly timescale. We focus on daytime measurements, since nighttime values of sensible and latent heat fluxes are low on a daily timescale. We separate upwinds and downwinds, following Zitouna-Chebbi et al. (2012). For plots A and B, the downwinds belong to the northwest sector (wind direction greater than 220 and less than 70°) while the upwinds belong to the south sector (wind direction between 135° and 225°). The reverse is true for plot C, namely downwinds belong to the south sector while upwinds belong to the northwest sector. East winds are disregarded, due to the position of the anemometer and the thermo-hygrometer (Zitouna-Chebbi et al., 2012). We also separate different intervals of vegetation, following Table 2 in Section 2.4.1, and in accordance to Zitouna-Chebbi et al. (2015).

When dealing with datasets A04 and C06, we setup a gap filling strategy for the time series of convective flux data H and LE, on the basis of (1) linear regressions between corrected and non-corrected convective fluxes, and (2) linear regressions between corrected convective fluxes and net radiation. When dealing with datasets B05 and A06, no

convective LE flux are available. We therefore apply the above-mentioned gap-filling strategy on sensible heat flux H only, and we estimate latent heat flux as the residual of surface energy balance. More details are given in Supplementary materials - Section 1 for gap filling methodology and Supplementary materials - Section 2 for gap filling performances.

## 3. Results and discussions

We report and discuss the results we obtain for temporal dynamics of energy fluxes and related ratios, including ratio of net radiation to solar irradiance, Bowen ratio, as well as ratio of actual to reference evapotranspiration. In most cases, we address the daily timescale and the annual extent, in order to capture temporal dynamics in relation to vegetation development stages and hydrometeorological conditions throughout several seasons. Also, we analyse and discuss ratios of energy fluxes according to upwinds and downwinds, since the influence of meteorological conditions related to northwest and south winds (Section 2.4.2) is mitigated for ratios as compared to fluxes.

### 3.1. Temporal dynamics of daily energy fluxes

Fig. 3 displays, for each of the four datasets A04, B05, A06 and C06, the seasonal variations of daytime energy fluxes at the daily timescale, including net radiation (Rn), soil heat flux (G), sensible and latent heat flux (H and LE). LE flux magnitude is displayed in both W m$^{-2}$ (left axis)
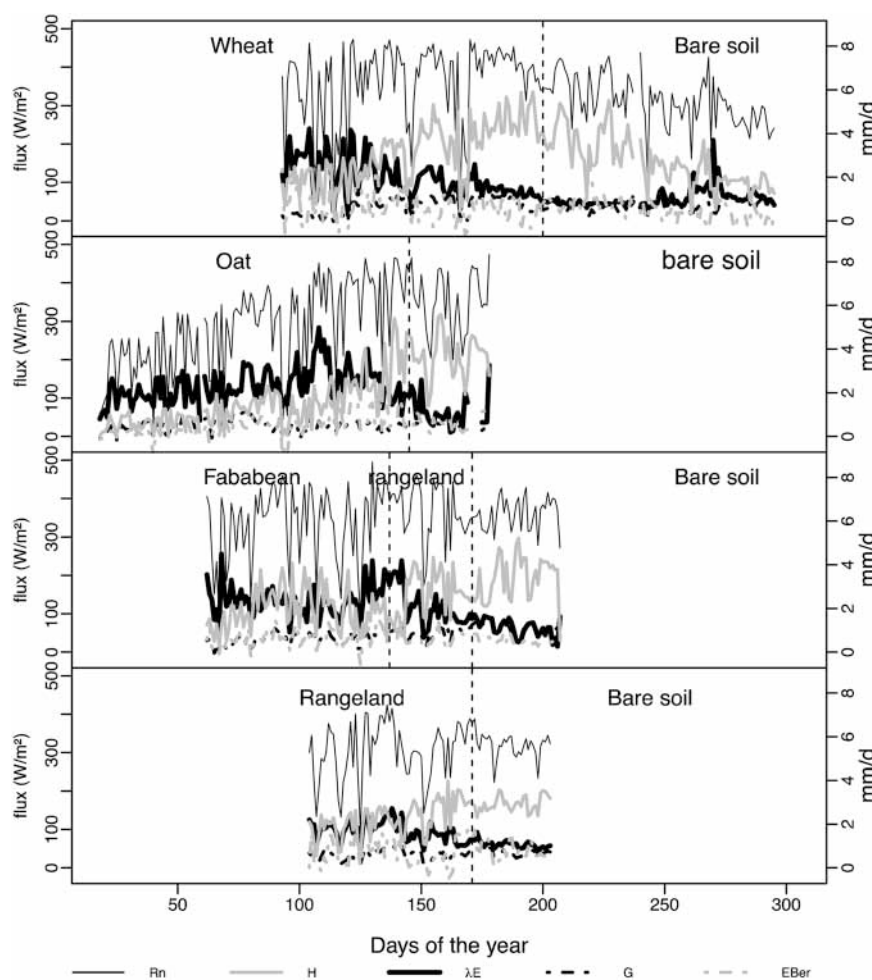


**Fig. 3.** Times series of daily fluxes, including net radiation, soil heat flux, sensible and latent heat flux, along with energy balance residue (EB_res), for datasets A04 (top), B05 (middle top), A06 (middle bottom) and C06 (bottom). The dashed lines indicate the harvest days (senescence on rangeland). Fluxes are scaled in W m$^{-2}$ (respectively mm day$^{-1}$) on the left axis (respectively right axis).

and mm day$^{-1}$ (right axis). Fig. 3 also displays the seasonal variations of energy balance error residue (EB_res = Rn - G - H - LE) that is a proxy of uncertainties related to measurements and data processing, as well as a proxy of intrinsic limitations of energy balance closure.

Daily Rn does not exceed 500 W m$^{-2}$ for all seasons and datasets. It reaches maximum values in spring for the four datasets (A04, B05, A06 and C06), mainly during senescence (SE) stages, and depicts lower values in summer and autumn with bare soils. We observe minimal Rn values for dataset B05 until winter, around 240 W m$^{-2}$ on average. Additionally, the abrupt decreases in Rn we observe throughout the time series are ascribed to cloud coverage.

For the current study, daily soil heat flux depicts the lower magnitude, with values always below 100 W m$^{-2}$. It also depicts no seasonal variability and no increase during dry seasons. G corresponds to 5 % of Rn during full development (FD) stage of the wheat crop (dataset A04), and to 17 % of Rn during bare soil conditions (dataset A06).

Daily sensible heat flux does not exceed 300 W m$^{-2}$ over the four datasets, and it depicts clear seasonal variations. It increases from spring to reach a maximum in summer, and decreases thereafter. It is very low during winter for dataset B05, and it does not exceed 50 W m$^{-2}$ during the rainy periods. Overall, it is less than 40 % of Rn when vegetation is well developed and it is more than 60 % of Rn in summer with bare soil conditions.

Daily latent heat flux, which corresponds to actual evapotranspiration (ET), rarely exceeds 200 W m$^{-2}$ (4 mm day$^{-1}$), even when it exceeds sensible heat flux. It depicts seasonal patterns, with maximum values in spring, followed by decreases to zero in summer. Also, it increases after each rain event. During the mid-development (MD) stages of barley and faba bean crops, LE corresponds to 50 % and 44 % of Rn. During the FD stages of wheat, barley, faba bean and rangeland, it corresponds to 44 %, 55 %, 38 % and 38 % of Rn, respectively. During the senescence stages, it corresponds to 25 %, 36 %, 32 % and 29 % of Rn, respectively. We also observe lower values for bare soil conditions, where LE corresponds to 14 %, 18 %, 19 % and 24 % of Rn, respectively. Additionally, we observe an increase up to 25 % of Rn for bare soil in autumn (dataset A04), which is ascribed to rain events.
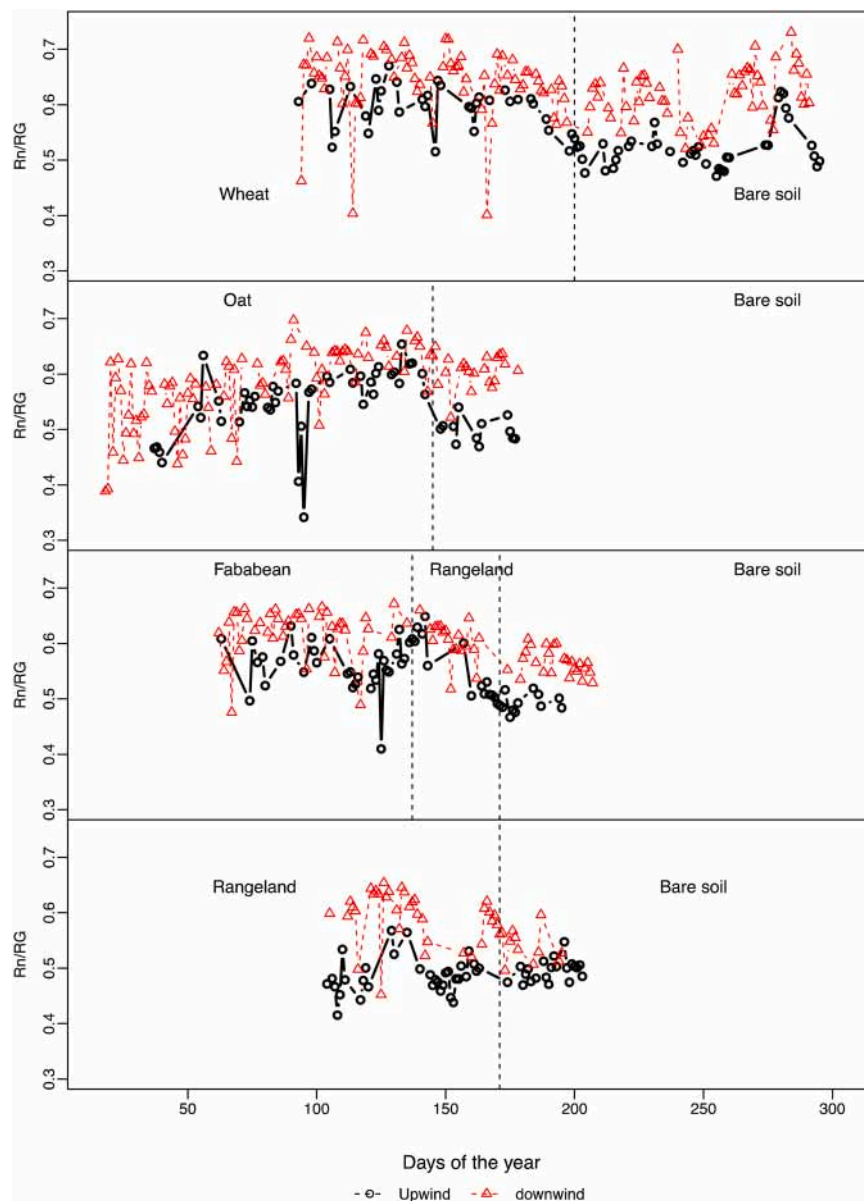


**Fig. 4.** Times series of daily values for the ratio Rn/Rg throughout the experimental periods according to upwinds and downwinds, for datasets A04 (top), B05 (middle top), A06 (middle bottom) and C06 (bottom). Upwinds (respectively downwinds) correspond to south winds for datasets A04, B05 and A06 (respectively C06), and to northwest winds for dataset C06 (respectively A04, B05 and A06).

Daily value of energy balance residual (EB_res) reaches up to 100 W m$^{-2}$ in some cases (dataset A04). It is close to H and G at the beginning of the time series for dataset B05, and it has the same magnitude than G and LE during the summer for all datasets. It represents between 6 % and 14 % of Rn during MD stage for dataset B05 and FD stage for dataset A04, respectively. Overall, high values of G/Rn are often accompanied by low values of EB_res/Rn.

Finally, we note that energy fluxes Rn, H, LE are lower for dataset C06, as compared to the three other datasets A04, b05 and A06. Besides, times series show simultaneous decreases and increases of the fluxes, which confirms the consistency between the independent measurements of the four energy balance components (Rn, G, H, LE).

### 3.2. Seasonal variations of daily Rn/Rg

To analyse the partitioning of daily energy fluxes under the specific conditions we address here, namely rainfed annual crops within Mediterranean hilly agrosystems, we study the temporal dynamic of net radiation to solar irradiance (Rn/Rg) at the daily time scale. This ratio is a proxy of the solar irradiance amount to be transformed into net radiation and subsequently into soil heat flux and convective fluxes (Ryu et al., 2008). Also, this ratio permits to quantify changes in net radiation Rn according to upwinds and downwinds, while attenuating the impact of changes in Rg between northwest and south winds (Section 2.4.2).

The ratio Rn/Rg shows a large variability from 0.35 to 0.7 (Fig. 4). First, we note some differences between upwinds and downwinds. These differences, between 0.04 and 0.12 on average, are observed for all plots, all years and throughout all experimental periods. The ratio Rn/ Rg is larger for downwinds (northwest winds for datasets A04, B05 and A06; south winds for dataset C06) as compared to upwinds (south winds for datasets A04, B05 and A06; northwest winds for dataset C06). Second, we note some differences from the viewpoint of vegetation development. The ratio Rn/Rg depicts largest values (0.59 on average) during the full development (FE) and senescence (SE) stages, and lowest values (0.55 on average) during bare soil conditions. Third, the temporal dynamics depicts seasonalities. The ratio Rn/Rg increases during autumn with the first rainfall for dataset A04, and it is smaller in winter than in spring for dataset B05. Indeed, the partitioning of the ratio Rn/Rg
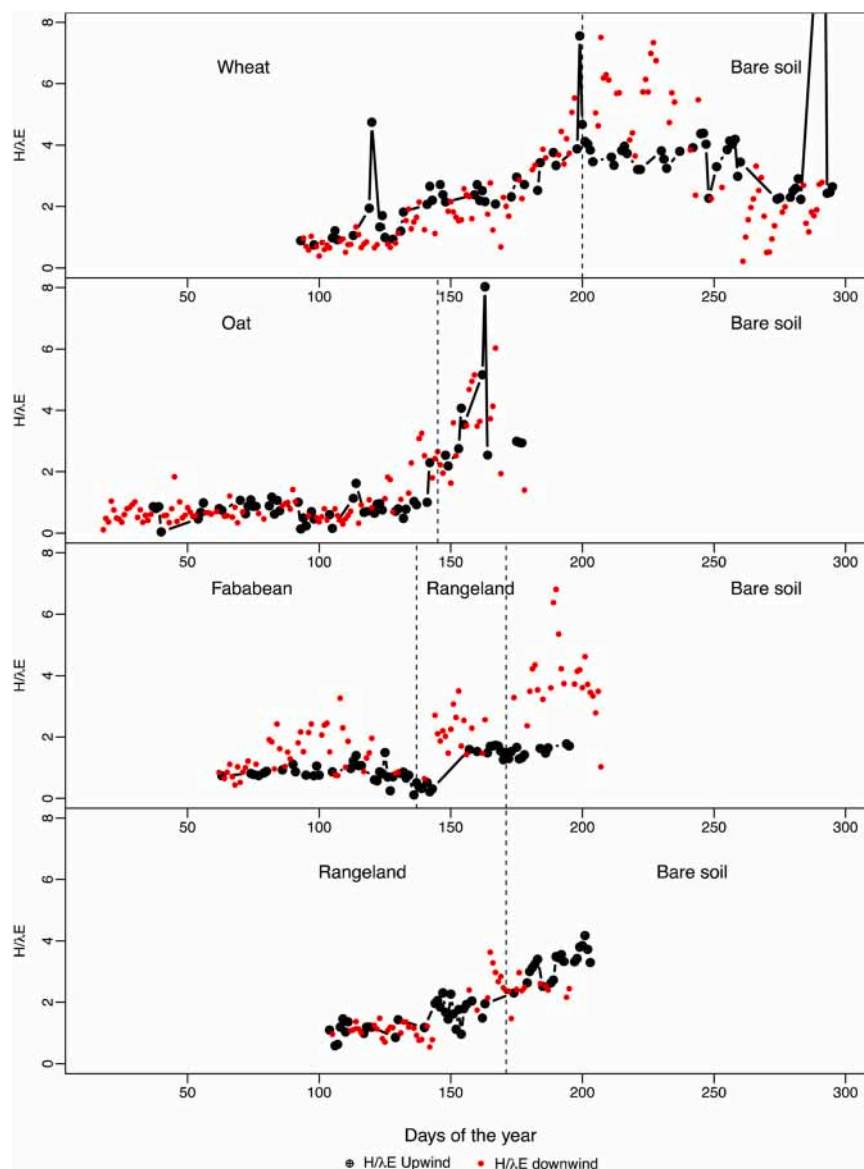


**Fig. 5.** Times series of daily values for the Bowen ratio H/LE throughout the experimental periods according to upwinds and downwinds, for datasets A04 (top), B05 (middle top), A06 (middle bottom) and C06 (bottom). Upwinds (respectively downwinds) correspond to south winds for datasets A04, B05 and A06 (respectively C06), and to northwest winds for dataset C06 (respectively A04, B05 and A06).

depends upon land cover and surface humidity, with larger values for humid and green covered surfaces.

### 3.3. Seasonal variation of daily Bowen ratio

The ratio H/LE is known as Bowen Ratio (BR) and is a proxy of water status (Perez et al., 2008). We analyse its temporal dynamic according to upwinds/downwinds, by assuming that ratioing the two convective fluxes mitigates the influence of meteorological conditions between northwest and south winds (Section 2.4.2).

We observe a clear variability during the experimental periods for the four datasets (Fig. 5). It varies from less than one to more than four. Across all datasets, it is lower than one during the mid-development (MD) stages and the full-development (FD) stages. It depicts the lowest values during the FD stage for dataset B05, with an average value of 0.53. It increases during the senescence (SE) stage, with an average value of 1.57, and increases up to more than 2 during the bare soil periods. For the dataset A06, it depicts an abrupt increase as compared to gradual increases for the other datasets. It depicts significant fluctuations during dry summer, which is ascribed to small variations in LE flux near zero. Finally, it changes according to upwinds and downwinds for dataset A06, with larger values for downwinds (northwest winds).

### 3.4. Seasonal variation of daily $ET/ET_0$

Fig. 6 displays the temporal variations of $ET/ET_0$ (ratio of actual to reference evapotranspiration) for the four datasets, by separating up-winds and downwinds. Additionally, subplots in Fig. 5 indicate the vegetation growth stages as determined by the measurements of LAI and plant height (Section 2.4.1).

Dataset A04 spreads over the FD and SE stages of the wheat crop, for which we indicate the average values of rainfall (1.3 and 0.4 mm day$^{-1}$), $ET_0$ (2.7 and 5.1 mm day$^{-1}$), ET (2.2 and 1.7 mm day$^{-1}$), EB_res (0.5 and 0.7 mm day$^{-1}$) and LAI_max (0.8 m$^2$ m$^2$). The ratio $ET/ET_0$ is stable throughout the FD stage, with an average value around 0.84. Then, it decreases during the SE stage down to 0.13 at the harvest period, and next increases to around 0.4 after the first autumn rainfall. Finally, $ET/ET_0$ is larger for downwinds (northwest winds) than for upwinds (south winds), with differences about 0.45 and 0.12 on average for FD and SE, respectively.

Dataset B05 spreads over the MD, FD and SE stages of the oat crop, for which we indicate the average values of rainfall (3.5, 2.5, and 0.5 mm day$^{-1}$), $ET_0$ (1.9, 2.5, and 4.3 mm day$^{-1}$), ET (1.4, 2.3, and 2.2 mm day$^{-1}$) and EB_res (0.2, 0.4, and 0.8 mm day$^{-1}$) and LAI_max (3 m$^2$ m$^2$). $ET/ET_0$ is lower than 0.5 during the MD stage, with peaks above unity after rain events. It next increases until the middle of the MD stage, and is then typified by a stress period (i.e., decrease) until the end
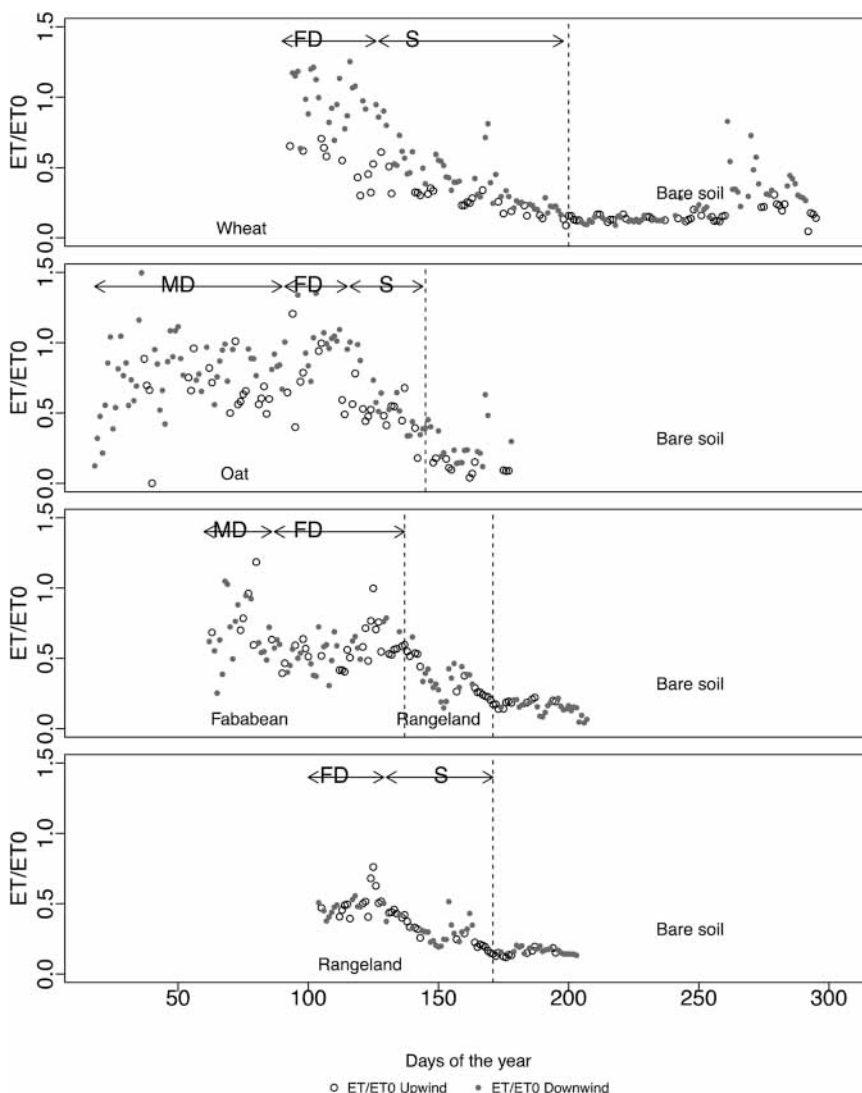


**Fig. 6.** Times series of daily values for the ratio $ET/ET_0$, throughout the experimental periods according to upwinds and downwinds, for datasets A04 (top), B05 (middle top), A06 (middle bottom) and C06 (bottom), and for different vegetation development stages (MD for mid-development, FD for full development stage, S for senescence). Upwinds (respectively downwinds) correspond to south winds for datasets A04, B05 and A06 (respectively C06), and to northwest winds for dataset C06 (respectively A04, B05 and A06).

of the MD stage. Indeed, cumulated rainfall is larger than cumulated $ET_0$ on average during the MD stage, but it is unequally distributed (Fig. SP4). Thus, rainfall amounts are large at the beginning of the MD stage, whereas both $ET_0$ and LAI are low. The subsequent soil water storage is large at the beginning of the MD period, for the benefit of vegetation growth, but it vanishes with time. During the FD stage, we observe a stress event, after which the ratio $ET/ET_0$ is stabilised around unity. Next, the SE period is typified by a decrease of $ET/ET_0$ down to 0.4 at the harvest time. We observe non negligible $ET/ET_0$ value after harvest, which indicates that vegetation is still active, conversely to what is observed for the wheat crop (dataset A04). Finally, the ratio $ET/ET_0$ is larger for downwinds (northwest winds) than for upwinds (south winds), with differences about 0.15, 0.24 and 0.08 on average for MD, FD and SE stages, respectively.

Dataset A06 spreads over the MD and FD stages of the faba bean crop, as well as over the following rangeland period, for which we indicate the average values of rainfall (1.3, 0.9 and 0.4 mm day$^{-1}$), $ET_0$ (2.6, 3.7 and 5.5 mm day$^{-1}$), ET (1.8, 2, and 1.9 mm day$^{-1}$), EB_res (0.4, 0.6 and 0.7 mm day$^{-1}$) and LAI_max (1.3 m$^2$ m$^2$). The ratio $ET/ET_0$ is slightly larger during the MD stage (0.69) than during the FD stage (0.56), which is explained by the lack of rainfall during the FD period. The rangeland period is typified by an average value of 0.35 for $ET/ET_0$, with a decrease trend on the first half, and an increase trend at the beginning of the second part that start after a 10 mm rainfall. Finally, the ratio $ET/ET_0$ is similar for upwinds and downwinds, where $ET/ET_0$ is slightly larger for upwinds (south winds) as compared to downwinds (northwest), with differences about 0.06 on average for MD.

Dataset C06 spreads over FD and SE stages of the rangeland, for which we indicate the average values of rainfall (1.5 and 0.8 mm day$^{-1}$), $ET_0$ (3.3 and 5.4 mm day$^{-1}$), ET (1.6 and 1.5 mm day$^{-1}$), EB_res (0.51 and 0.67 mm day$^{-1}$) and LAI_max (0.9 m$^2$ m$^2$). During the FD stage, the ratio $ET/ET_0$ is relatively stable with an average value of 0.5, and it decreases during the SE stage down to 0.2, with an average value of 0.3 over the SE stage. The ratio $ET/ET_0$ is lower for upwinds (northwest winds) as compared to the downwinds (south winds), with differences about 0.07 and 0.05 respectively for FD and SE.

On the basis of the results reported and discussed across the four datasets A04, B05, A06 and C06, we highlight general outcomes, listed below.

- For the bare soil periods, the ratio $ET/ET_0$ corresponds to an evaporation term. It is lower than 0.2 only until the end of the experimental periods for dataset A04, except after the autumnal rainfalls where it reaches values close to unity. Across all datasets, periods with water loss from evaporation are observed during the autumn season or at the beginning of the MD period.
- The maximum values we observe for the ratio $ET/ET_0$ are lower than 1.2. This threshold value is consistent with the interval suggested by Allen et al. (2011). We note that adding EB_res to LE fluxes, which corresponds to the most pessimistic case, would lead to a maximum value for $ET/ET_0$ that does not exceed 1.5, which is still within the aforementioned interval.
- All times series for the ratio $ET/ET_0$ clearly depict seasonal behaviours, despite fluctuations that are ascribed to temporal changes in water supply for rainfed annual crops. Across the four datasets, we observe rapid and systematic decreases of ET when $ET_0$ is larger than 4 mm day$^{-1}$, where the latter seems to be a threshold value for vegetation transpiration. This systematic and rapid decrease of ETR / $ET_0$ may be explained by two driving factors, namely vegetation senescence and decrease of water content, these two driving factors being linked because of water shortage. Thus, decrease in ETR induced increase of the temperature of the vegetation, and thus acceleration of phenology that is driven by cumulated temperature (Sacks and Kucharik, 2011).

The faba bean crop depict vegetation growth similar to that reported

by Manschadi et al. (1998) in Mediterranean conditions. In conditions similar to those of our study, for water limited case and late sowing (December), they report that ET is lower but water use efficiency is larger than for well-watered conditions.

## 4. Discussion

Our observations for the temporal dynamics of daily energy fluxes are consistent with previous studies in similar contexts, either Mediterranean or semi-arid. (1) Rn is low over dry vegetation/bare soil without evapotranspiration, since larger albedo values induce decreases in shortwave radiation that drives net radiation by 60–80 %, while larger surface temperature values induce decrease in longwave radiation (Jacob et al., 2002; Ryu et al., 2008). (2) For the same reason, Rn is slightly larger over covering crops like wheat and slightly lower over sparse vegetation like rangeland. (3) Only G does not depict any seasonal pattern, as previously observed by Wang et al. (2010), and it is quite similar regardless of crop. (4) The magnitude of ET is less than 4 mm day$^{-1}$ over the four growth cycles of rainfed vegetation we consider here, and it corresponds to 60 % of Rn at most, which is moderately lower than the LE/Rn ratio of 85 % reported during the growing season of grassland by Ryu et al. (2008). (5) The partition between H and LE we observe here is similar to that reported by Wang et al. (2010). This is consistent with the seasonal variations of the energy balance components, where sensible (respectively latent) heat flux is the main consumer of available energy in summer and autumn (respectively winter and spring). (6) The magnitude of LE is slightly larger over covering crops like wheat and slightly lower over sparse vegetation like rangeland, since soil moisture decreases faster than root zone moisture (Galleguillos et al., 2017; Montes et al., 2014). (7) Regardless of crop, H is larger than LE after day 140–150 because of water shortage, which is typical of water-driven processes. (7) The magnitude of EB_res is close to that of G, and it varies similarly to G. Possible explanations are related to available energy and soil thermal conductivity that are driven by vegetation fraction cover that depends on phenological stage, and by seasonal dynamics of soil moisture. Then, it is expected that correcting soil heat flux could improve energy balance ratio. Indeed, Wang et al. (2010) improved energy balance ratio (H + LE)/(Rn-G) from 0.78 to 0.86, by correcting the soil heat flux for heat storage. Also, Franssen et al. (2010) stated that a 20 W m$^{-2}$ non-closure of energy balance can be attributed to measurement errors and/or neglected storage terms. However, we recall that existing corrections are questionable for the swelling soils we consider here (Section 2.5). (8) Finally, the time series we observe over rainfed annual crops are notably different from those reported over irrigated annual crops by Payero and Irmak (2013), with larger values for H and lower values for LE in our case.

We report here larger values for the ratio Rn/Rg, as compared to those reported by Ryu et al. (2008) for Mediterranean grasslands and for several FLUXNET sites. This indicates that incoming solar energy is more efficiently converted into available energy for the sites we consider in the current study. Also, we note that the changes in ratio Rn/Rg we observe according to upwinds and downwinds has not been reported by any study in the literature, to our best knowledge.

As compared to previous studies, we obtain consistent values of Bowen ratio for different periods throughout our times series, namely winter, end of spring with water stress, summer with vegetation drying, and bare soil (Mamadou et al., 2014). However, we cannot draw any conclusion, since we found in the literature only one report on such long time series. Also, we note that our time series are not consistent anymore when assuming all measurement errors on LE (no energy balance error residue), since BR does not depict any stress event during drying periods. This indicates that measurements errors do not affect LE data only (data not shown).

The largest value we observe for the ratio $ET/ET_0$ during the winter does not correspond to large values of ET, because $ET_0$ is low in winter. This season, which is energy limited, is on contrary typified by large

rainfalls that are not directly used by vegetation and that are distributed between infiltration and runoff. Thus, the rainfall distribution between green and blue water is a significant concern in hilly Mediterranean catchments, for better water management modes in context of water scarcity (Mekki et al., 2006). Looking for technical practices strategies is therefore important. In fact, for wheat and oat, the uniform row pattern plantation is a classical technical practice. Quanqi et al. (2012) reported that in semi-arid areas, water use efficiency for wheat crops is larger when using furrow and bed planting patterns by 13 % and 6 %, respectively, as compared to the use of uniform row planting pattern.

For all ratios of energy fluxes, namely the ratio of net radiation to solar irradiance (Rn/Rg), the Bowen Ratio (BR), as well as the ratio of actual to reference evapotranspiration ($ET/ET_0$), we observe some differences between upwinds and downwinds, in agreement with former experimental reports by Zitouna-Chebbi et al. (2015, 2012). Rn/Rg and Bowen ratio are systematically larger for downwinds, as compared to upwinds, whereas this trend is not systematic for $ET/ET_0$. Also, the differences between upwinds and downwinds have a magnitude that is comparable to the energy balance residual (EB_res), while ET is reconstructed as energy balance residual for dataset B05 and A06. These elements make any conclusion questionable, and further works are necessary. A possible line of investigation is the change of aerodynamic conditions (roughness length) that drive convective fluxes, because of airflow streamline dilatation and contraction, as reported numerically and analytically by Belcher et al. (1993), Raupach and Finnigan (1997).

## 5. Conclusion

The current study aims to document evapotranspiration and related surface energy fluxes for rainfed annual crops within a Mediterranean hilly agrosystem, by considering the plot scale within a case study located in the Cap Bon peninsula, north-eastern Tunisia.

We report on seasonal variability of daily evapotranspiration and surface energy fluxes, as well as on seasonal variability of several proxies that document vegetation water status (flux ratios Rn/Rg, H/LE and $ET/ET_0$), by considering daily timescale and annual extent in relation to crop phenology and hydrometeorological conditions. It is shown that (1) our time series of energy fluxes show classical seasonal dynamics, (2) our observations are consistent with previous studies in Mediterranean or semi-arid contexts, and (3) our observations are notably different from those reported over irrigated annual crops. For flux ratios, we observe changes according to upwinds and downwinds, although the magnitudes of these changes are within the energy balance residual. Further investigations are therefore necessary, such as possible changes in aerodynamic conditions because of streamline dilatation/contraction, in accordance to upwinds and downwinds.

Overall, we state that EC measurements are promising over rainfed annual crops within semiarid hilly agrosystems, for long term observations, environmental modelling and operational purposes. Thus, the current study provides a database of energy flux observations that can be used to calibrate or validate various models dealing with land surface processes for agricultural water management. This study also provides some insights about the identification of energy-limited and water-limited periods for different crops growth cycles, where climate forcing is more important than eco-physiological differences between crops. Thus, it seems that an $ET_0$ value of 4 mm day$^{-1}$ is a threshold beyond which ET decreases systematically and rapidly, at least for the four crops included in our study case.

Additionally, we recommend to practitioners the setting up of a wind direction sensor within any agrometeorological station when dealing with hilly agrosystems, so that any experimental correction can be further tailored by accounting for the combination of topography and wind direction. In terms of agricultural water management, the current study suggests to look for early sowing species/varieties, in order to reduce the evaporation-based water loss in autumn. It also suggests to explore supplemental irrigation during the critical phenological stages

with water shortages.

Finally, the current study is conducted over few small fields within a specific hilly topography. The results we report here are new, and they need to be strengthened with additional experiments, for a better understanding of the underlying processes such as changes in solar radiation with slope orientation, changes in soil depth, soil moisture and vegetation growth, as well as changes in convective fluxes because of various factors (air streamlines within the boundary layer, aerodynamic and micrometeorological conditions, source contributions).

## Declaration of Competing Interest

The authors declare that they have no known competing financial interests or personal relationships that could have appeared to influence the work reported in this paper.

## Data Availability

Data will be made available on request.

## Appendix A. Supporting information

Supplementary data associated with this article can be found in the online version at doi:10.1016/j.agwat.2022.108117.

## References

Al-Khuzaie, M.M., Janna, H., Al-Ansari, N., 2020. Assessment model of water harvesting and storage location using GIS and remote sensing in Al-Qadisiyah, Iraq. Arab. J. Geosci. 13, 1154. https://doi.org/10.1007/s12517-020-06154-4.

Allen, R.G., Pereira, L.S., Raes, D., Smith, M., 1998. Crop Evapotranspiration-guidelines for Computing Crop Water Requirements-FAO Irrigation and Drainage Paper 56, 300. Fao, Rome, p. D05109.

Allen, R.G., Pereira, L.S., Howell, T.A., Jensen, M.E., 2011. Evapotranspiration information reporting: II. Recommended documentation. Agric. Water Manag. 98, 921–929. https://doi.org/10.1016/j.agwat.2010.12.016.

Ammar, A., Riksen, M., Ouessar, M., Ritsema, C., 2016. Identification of suitable sites for rainwater harvesting structures in arid and semi-arid regions: a review. Int. Soil Water Conserv. Res. 4, 108–120. https://doi.org/10.1016/j.iswcr.2016.03.001.

Anapalli, S.S., Fisher, D.K., Pinnamaneni, S.R., Reddy, K.N., 2020. Quantifying evapotranspiration and crop coefficients for cotton (Gossypium hirsutum L.) using an eddy covariance approach. Agric. Water Manag. 233, 106091 https://doi.org/10.1016/j.agwat.2020.106091.

Aouade, G., Jarlan, L., Ezzahar, J., Er-Raki, S., Napoly, A., Benkaddour, A., Khabba, S., Boulet, G., Garrigues, S., Chehbouni, A., Boone, A., 2020. Evapotranspiration partition using the multiple energy balance version of the ISBA-A-gₛ land surface model over two irrigated crops in a semi-arid Mediterranean region (Marrakech, Morocco). Hydrol. Earth Syst. Sci. 24, 3789–3814. https://doi.org/10.5194/hess-24-3789-2020.

Aubinet, M., Vesala, T., Papale, D. (Eds.), 2012. Eddy Covariance: A Practical Guide to Measurement and Data Analysis. Springer, Netherlands, Dordrecht. https://doi.org/10.1007/978-94-007-2351-1.

Belcher, S.E., Newley, T.M.J., Hunt, J.C.R., 1993. The drag on an undulating surface induced by the flow of a turbulent boundary layer. J. Fluid Mech. 249, 557. https://doi.org/10.1017/S0022112093001296.

Boudhina, N., Masmoudi, M.M., Ben Mechlia, N., Zitouna, R., Mekki, I., Prévot, L., Jacob, F., 2017. Evapotranspiration of wheat in a hilly topography: results from measurements using a set of Eddy covariance stations. In: Ouessar, M., Gabriels, D., Tsunekawa, A., Evett, S. (Eds.), Water and Land Security in Drylands. Springer

International Publishing, Cham, pp. 67–76. https://doi.org/10.1007/978-3-319-54021-4_7.

Boudhina, N., Masmoudi, M.M., Jacob, F., Prévot, L., Zitouna-Chebbi, R., Mekki, I., Ben Mechlia, N., 2018a. Measuring crop evapotranspiration over hilly areas. In: Kallel, A., Ksibi, M., Ben Dhia, H., Khélifi, N. (Eds.), Recent Advances in Environmental Science from the Euro-Mediterranean and Surrounding Regions, Advances in Science, Technology & Innovation. Springer International Publishing, Cham, pp. 909–911. https://doi.org/10.1007/978-3-319-70548-4_266.

Boudhina, N., Zitouna-Chebbi, R., Mekki, I., Jacob, F., Ben Mechlia, N., Masmoudi, M., Prévot, L., 2018b. Evaluating four gap-filling methods for eddy covariance measurements of evapotranspiration over hilly crop fields. Geosci. Instrum. Methods Data Syst. 7, 151–167. https://doi.org/10.5194/gi-7-151-2018.

Boudhina, N., Masmoudi, M.M., Alaya, I., Jacob, F., Ben Mechlia, N., 2019. Use of AquaCrop model for estimating crop evapotranspiration and biomass production in hilly topography. Arab. J. Geosci. 12, 259. https://doi.org/10.1007/s12517-019-4434-9.

Brouzyne, Y., Abouabdillah, A., Hirich, A., Bouabid, R., Zaaboul, R., Benaabidate, L., 2018. Modeling sustainable adaptation strategies toward a climate-smart agriculture in a Mediterranean watershed under projected climate change scenarios. Agric. Syst. 162, 154–163. https://doi.org/10.1016/j.agsy.2018.01.024.

Chakraborty, A., Choudhary, K.K., Srikanth, P., Ramana, K.V., Seshasai, M.V.R., Narayanarao, K., Amaregouda, A., Yadav, Y., Annapurna, G., 2021. $CO_2$, $H_2O$ and energy fluxes from chickpea crop grown under residual soil moisture condition in rainfed peninsular India using eddy covariance techniques. Field Crops Res. 273, 108307 https://doi.org/10.1016/j.fcr.2021.108307.

Chen, B., Chamecki, M., Katul, G.G., 2019. Effects of topography on in-canopy transport of gases emitted within dense forests. Q J. R. Meteorol. Soc. 145, 2101–2114. https://doi.org/10.1002/qj.3546.

Cheng, M., Jiao, X., Shi, L., Penuelas, J., Kumar, L., Nie, C., Wu, T., Liu, K., Wu, W., Jin, X., 2022. High-resolution crop yield and water productivity dataset generated using random forest and remote sensing. Sci. Data 9, 641. https://doi.org/10.1038/s41597-022-01761-0.

Dare-Idowu, O., Jarlan, L., Le-Dantec, V., Rivalland, V., Ceschia, E., Boone, A., Brut, A., 2021. Hydrological functioning of maize crops in Southwest France using Eddy covariance measurements and a land surface model. Water 13, 1481. https://doi.org/10.3390/w13111481.

Dhouib, M., Zitouna-Chebbi, R., Prévot, L., Molénat, J., Mekki, I., Jacob, F., 2022. Multicriteria evaluation of the AquaCrop crop model in a hilly rainfed Mediterranean agrosystem. Agric. Water Manag. 273, 107912 https://doi.org/10.1016/j.agwat.2022.107912.

Elbeltagi, A., Deng, J., Wang, K., Malik, A., Maroufpoor, S., 2020. Modeling long-term dynamics of crop evapotranspiration using deep learning in a semi-arid environment. Agric. Water Manag. 241, 106334 https://doi.org/10.1016/j.agwat.2020.106334.

Finnigan, J., Harman, I., Ross, A., Belcher, S., 2015. First-order turbulence closure for modelling complex canopy flows: first-order turbulence closure for canopy flows. Q. J. R. Meteorol. Soc. 141, 2907–2916. https://doi.org/10.1002/qj.2577.

Foken, T., Göockede, M., Mauder, M., Mahrt, L., Amiro, B., Munger, W., 2005. Post-field data quality control. In: Lee, X., Massman, W., Law, B. (Eds.), Handbook of Micrometeorology, Atmospheric and Oceanographic Sciences Library. Kluwer Academic Publishers, Dordrecht, pp. 181–208. https://doi.org/10.1007/1-4020-2265-4_9.

Foken, Th., Wichura, B., 1996. Tools for quality assessment of surface-based flux measurements. Agric. For. Meteorol. 78, 83–105. https://doi.org/10.1016/0168-1923(95)02248-1.

Franssen, H.J.H., Stöckli, R., Lehner, I., Rotenberg, E., Seneviratne, S.I., 2010. Energy balance closure of eddy-covariance data: a multisite analysis for European FLUXNET stations. Agric. For. Meteorol. 150, 1553–1567. https://doi.org/10.1016/j.agrformet.2010.08.005.

French, A.N., Hunsaker, D.J., Sanchez, C.A., Saber, M., Gonzalez, J.R., Anderson, R., 2020. Satellite-based NDVI crop coefficients and evapotranspiration with eddy covariance validation for multiple durum wheat fields in the US Southwest. Agric. Water Manag. 239, 106266 https://doi.org/10.1016/j.agwat.2020.106266.

Galleguillos, M., Jacob, F., Prévot, L., Faúndez, C., Bsaibes, A., 2017. Estimation of actual evapotranspiration over a rainfed vineyard using a 1-D water transfer model: a case study within a Mediterranean watershed. Agric. Water Manag. 184, 67–76. https://doi.org/10.1016/j.agwat.2017.01.006.

Gaubi, I., Chaabani, A., Ben Mammou, A., Hamza, M.H., 2017. A GIS-based soil erosion prediction using the Revised Universal Soil Loss Equation (RUSLE) (Lebna watershed, Cap Bon, Tunisia). Nat. Hazards 86, 219–239. https://doi.org/10.1007/s11069-016-2684-3.

Grum, B., Assefa, D., Hessel, R., Woldearegay, K., Ritsema, C.J., Aregawi, B., Geissen, V., 2017. Improving on-site water availability by combining in-situ water harvesting techniques in semi-arid Northern Ethiopia. Agric. Water Manag. 193, 153–162. https://doi.org/10.1016/j.agwat.2017.08.009.

Hammerle, A., Haslwanter, A., Schmitt, M., Bahn, M., Tappeiner, U., Cernusca, A., Wohlfahrt, G., 2007. Eddy covariance measurements of carbon dioxide, latent and sensible energy fluxes above a meadow on a mountain slope. Bound.-Layer. Meteorol. 122, 397–416. https://doi.org/10.1007/s10546-006-9109-x.

Harmanny, K.S., Malek, Ž., 2019. Adaptations in irrigated agriculture in the Mediterranean region: an overview and spatial analysis of implemented strategies. Reg. Environ. Change 19, 1401–1416. https://doi.org/10.1007/s10113-019-01494-8.

Hiller, R., Zeeman, M.J., Eugster, W., 2008. Eddy-covariance flux measurements in the complex terrain of an Alpine Valley in Switzerland. Bound.-Layer. Meteorol. 127, 449–467. https://doi.org/10.1007/s10546-008-9267-0.

Holst, T., Rost, J., Mayer, H., 2005. Net radiation balance for two forested slopes on opposite sides of a valley. Int. J. Biometeorol. 49, 275–284. https://doi.org/10.1007/s00484-004-0251-1.

Hossain, A., Sab, A.E., Barutcular, C., Bhatt, R., Cig, F., Seydosoglu, S., Turan, N., Konuskan, O., Iqbal, M.A., Abdelhamid, M., Soler, C.M.T., Laing, A.M., Saneoka, H., 2020. Sustainable crop production to ensuring food security under climate change: a Mediterranean perspective. Aust. J. Crop Sci. 14, 439–446. https://doi.org/10.3316/informit.121077065862236.

Jacob, F., Olioso, A., Gu, X.F., Su, Z., Seguin, B., 2002. Mapping surface fluxes using airborne visible, near infrared, thermal infrared remote sensing data and a spatialized surface energy balance model. Agronomie 22, 669–680. https://doi.org/10.1051/agro:2002053.

Jarlan, L., Khabba, S., Er-Raki, S., Le Page, M., Hanich, L., Fakir, Y., Merlin, O., Mangiarotti, S., Gascoin, S., Ezzahar, J., Kharrou, M.H., Berjamy, B., Saaïdi, A., Boudhar, A., Benkaddour, A., Laftouhi, N., Abaoui, J., Tavernier, A., Boulet, G., Simonneaux, V., Driouech, F., El Adnani, M., El Fazziki, A., Amenzou, N., Raibi, F., El Mandour, A., Ibouh, H., Le Dantec, V., Habets, F., Tramblay, Y., Mougenot, B., Leblanc, M., El Faïz, M., Drapeau, L., Coudert, B., Hagolle, O., Filali, N., Belaqziz, S., Marchane, A., Szczypta, C., Toumi, J., Diarra, A., Aouade, G., Hajhouji, Y., Nassah, H., Bigeard, G., Chirouze, J., Boukhari, K., Abourida, A., Richard, B., Fanise, P., Kasbani, M., Chakir, A., Zribi, M., Marah, H., Naimi, A., Mokssit, A., Kerr, Y., Escadafal, R., 2015. Remote sensing of water resources in semi-arid Mediterranean areas: the joint international laboratory TREMA. Int. J. Remote Sens. 36, 4879–4917. https://doi.org/10.1080/01431161.2015.1093198.

Kanda, E.K., Senzanje, A., Mabhaudhi, T., 2021. Calibration and validation of the AquaCrop model for full and deficit irrigated cowpea (Vigna unguiculata (L.) Walp. Phys. Chem. Earth Parts A/B/C 124, 102941. https://doi.org/10.1016/j.pce.2020.102941.

Karrou, M., Oweis, T., 2012. Water and land productivities of wheat and food legumes with deficit supplemental irrigation in a Mediterranean environment. Agric. Water Manag. 107, 94–103. https://doi.org/10.1016/j.agwat.2012.01.014.

Lebon, N., Dagès, C., Burger-Leenhardt, D., Fabre, J.-C., Molénat, J., 2019. DAHM-Reservoir: an agro-hydrological model for agricultural catchment with small water reservoirs, 17006.

Liu, G., Liu, Y., Hafeez, M., Xu, D., Vote, C., 2012. Comparison of two methods to derive time series of actual evapotranspiration using eddy covariance measurements in the southeastern Australia. J. Hydrol. 454–455, 1–6. https://doi.org/10.1016/j.jhydrol.2012.05.011.

Longobardi, A., Villani, P., 2013. The use of micrometeorological data to identify significant variables in evapotranspiration modeling. Procedia Environ. Sci. 19, 267–274. https://doi.org/10.1016/j.proenv.2013.06.031.

Mamadou, O., Cohard, J.M., Galle, S., Awanou, C.N., Diedhiou, A., Kounouhewa, B., Peugeot, C., 2014. Energy fluxes and surface characteristics over a cultivated area in Benin: daily and seasonal dynamics. Hydrol. Earth Syst. Sci. 18, 893–914. https://doi.org/10.5194/hess-18-893-2014.

Manschadi, A.M., Sauerborn, J., Stützel, H., Göbel, W., Saxena, M.C., 1998. Simulation of faba bean (Vicia faba L.) growth and development under Mediterranean conditions: model adaptation and evaluation. Eur. J. Agron. 9, 273–293. https://doi.org/10.1016/S1161-0301(98)00045-8.

Mekki, I., Albergel, J., Ben Mechlia, N., Voltz, M., 2006. Assessment of overland flow variation and blue water production in a farmed semi-arid water harvesting catchment. Phys. Chem. Earth Parts A/B/C Assess. Water Qual. Catchment Scale 31, 1048–1061. https://doi.org/10.1016/j.pce.2006.07.003.

Mekki, I., Zitouna Chebbi, R., Jacob, F., Ben Mechlia, N., Prevot, L., Albergel, J., Voltz, M., 2018. Impact of land use on soil water content in a hilly rainfed agrosystem: a case study in the Cap Bon peninsula in Tunisia. Agrofor. Int. 3, 64–75. https://doi.org/10.7251/AGRENG1801064M.

Molénat, J., Raclot, D., Zitouna, R., Andrieux, P., Coulouma, G., Feurer, D., Grünberger, O., Lamachère, J.-M., Bailly, J.-S., Belotti, J.-L., Ben Azzez, K., Ben Mechlia, N., Ben Younès Louati, M., Biarnès, A., Blanca, Y., Carriere, D., Chaabane, H., Dagès, C., Debabria, A., Dubreuil, A., Fabre, J., Fages, D., Floure, C., Garnier, F., Geniez, C., Gomez, C., Hamdi, R., Huttel, O., Jacob, F., Jenhaoui, Z., Lagacherie, P., Le Bissonnais, Y., Louati, R., Louchart, X., Mekki, I., Moussa, R., Negro, S., Pépin, Y., Prévot, L., Samouëlian, A., Seidel, J.L., Trotoux, G., Troiano, S., Vinatier, F., Zante, P., Zrelli, J., Albergel, J., Voltz, M., 2018. OMERE: a long-term observatory of soil and water resources, in interaction with agricultural and land management in Mediterranean hilly catchments. Vadose Zone J. 17 https://doi.org/10.2136/vzj2018.04.0086.

Montes, C., Lhomme, J.-P., Demarty, J., Prévot, L., Jacob, F., 2014. A three-source SVAT modeling of evaporation: application to the seasonal dynamics of a grassed vineyard. Agric. For. Meteorol. 191, 64–80. https://doi.org/10.1016/j.agrformet.2014.02.004.

Nie, D., Demetriades-Shah, T., Kanemasu, E.T., 1992. Surface energy fluxes on four slope sites during FIFE 1988. J. Geophys. Res. 97, 18641. https://doi.org/10.1029/91JD03043.

Payero, J.O., Irmak, S., 2013. Daily energy fluxes, evapotranspiration and crop coefficient of soybean. Agric. Water Manag. 129, 31–43. https://doi.org/10.1016/j.agwat.2013.06.018.

Perez, P.J., Castellvi, F., Martínez-Cob, A., 2008. A simple model for estimating the Bowen ratio from climatic factors for determining latent and sensible heat flux. Agric. For. Meteorol. 148, 25–37. https://doi.org/10.1016/j.agrformet.2007.08.015.

Quanqi, L., Xunbo, Z., Yuhai, C., Songlie, Y., 2012. Water consumption characteristics of winter wheat grown using different planting patterns and deficit irrigation regime. Agric. Water Manag. 105, 8–12. https://doi.org/10.1016/j.agwat.2011.12.015.

Raclot, D., Albergel, J., 2006. Runoff and water erosion modelling using WEPP on a Mediterranean cultivated catchment. Phys. Chem. Earth Parts A/B/C Assess. Water Qual. Catchment Scale 31, 1038–1047. https://doi.org/10.1016/j.pce.2006.07.002.

Rafi, Z., Merlin, O., Le Dantec, V., Khabba, S., Mordelet, P., Er-Raki, S., Amazirh, A., Olivera-Guerra, L., Ait Hssaine, B., Simonneaux, V., Ezzahar, J., Ferrer, F., 2019. Partitioning evapotranspiration of a drip-irrigated wheat crop: inter-comparing eddy covariance-, sap flow-, lysimeter- and FAO-based methods. Agric. For. Meteorol. 265, 310–326. https://doi.org/10.1016/j.agrformet.2018.11.031.

Ran, H., Kang, S., Hu, X., Li, S., Wang, W., Liu, F., 2020. Capability of a solar energy-driven crop model for simulating water consumption and yield of maize and its comparison with a water-driven crop model. Agric. For. Meteorol. 287, 107955 https://doi.org/10.1016/j.agrformet.2020.107955.

Rana, G., Ferrara, R.M., Martinelli, N., Personnic, P., Cellier, P., 2007. Estimating energy fluxes from sloping crops using standard agrometeorological measurements and topography. Agric. For. Meteorol. 146, 116–133. https://doi.org/10.1016/j.agrformet.2007.05.010.

Rana, G., Katerji, N., Ferrara, R.M., Martinelli, N., 2011. An operational model to estimate hourly and daily crop evapotranspiration in hilly terrain: validation on wheat and oat crops. Theor. Appl. Clim. 103, 413–426. https://doi.org/10.1007/s00704-010-0308-5.

Raupach, M.R., Finnigan, J.J., 1997. The influence of topography on meteorological variables and surface-atmosphere interactions. J. Hydrol. 190, 182–213. https://doi.org/10.1016/S0022-1694(96)03127-7.

Ryu, Y., Baldocchi, D.D., Ma, S., Hehn, T., 2008. Interannual variability of evapotranspiration and energy exchange over an annual grassland in California. J. Geophys. Res. 113, D09104 https://doi.org/10.1029/2007JD009263.

Sacks, W.J., Kucharik, C.J., 2011. Crop management and phenology trends in the U.S. Corn Belt: impacts on yields, evapotranspiration and energy balance. Agric. For. Meteorol. 151, 882–894. https://doi.org/10.1016/j.agrformet.2011.02.010.

Schotanus, P., Nieuwstadt, F.T.M., De Bruin, H.A.R., 1983. Temperature measurement with a sonic anemometer and its application to heat and moisture fluxes. Bound.-Layer. Meteorol. 26, 81–93. https://doi.org/10.1007/BF00164332.

Serrano-Ortiz, P., Sánchez-Cañete, E.P., Olmo, F.J., Metzger, S., Pérez-Priego, O., Carrara, A., Alados-Arboledas, L., Kowalski, A.S., 2016. Surface-parallel sensor orientation for assessing energy balance components on mountain slopes. Bound.-Layer. Meteorol. 158, 489–499. https://doi.org/10.1007/s10546-015-0099-4.

Siad, S.M., Iacobellis, V., Zdruli, P., Gioia, A., Stavi, I., Hoogenboom, G., 2019. A review of coupled hydrologic and crop growth models. Agric. Water Manag. 224, 105746 https://doi.org/10.1016/j.agwat.2019.105746.

Talebizadeh, M., Moriasi, D., Gowda, P., Steiner, J.L., Tadesse, H.K., Nelson, A.M., Starks, P., 2018. Simultaneous calibration of evapotranspiration and crop yield in agronomic system modeling using the APEX model. Agric. Water Manag. 208, 299–306. https://doi.org/10.1016/j.agwat.2018.06.043.

Tromp-van Meerveld, H.J., McDonnell, J.J., 2006. On the interrelations between topography, soil depth, soil moisture, transpiration rates and species distribution at the hillslope scale. Adv. Water Resour. 29, 293–310. https://doi.org/10.1016/j.advwatres.2005.02.016.

Vadez, V., Pilloni, R., Grondin, A., Hajjarpoor, A., Belhouchette, H., Brouziyn, Y., Chehbouni, G., Kharrou, M.H., Zitouna-Chebbi, R., Mekki, I., Molénat, J., Jacob, F., Bossuet, J., 2022. Crop water use efficiency (WUE) and beyond. J. Exp. Bot. (submitted for publication).

Van Dijk, A., Moene, A.F., De Bruin, H.A.R., 2004. The Principles of Surface Flux Physics: Theory, Practice and Description of the ECPACK Library. Meteorology and Air Quality Group, Wageningen University, Wageningen, the Netherlands, p. 525.

Vickers, D., Mahrt, L., 1997. Quality control and flux sampling problems for tower and aircraft data. J. Atmos. Ocean. Technol. 14, 512–526. https://doi.org/10.1175/1520-0426(1997)014<0512:QCAFSP>2.0.CO;2.

Wang, G., Huang, J., Guo, W., Zuo, J., Wang, J., Bi, J., Huang, Z., Shi, J., 2010. Observation analysis of land-atmosphere interactions over the Loess Plateau of northwest China. J. Geophys. Res. 115, D00K17. https://doi.org/10.1029/2009JD013372.

Webb, E.K., Pearman, G.I., Leuning, R., 1980. Correction of flux measurements for density effects due to heat and water vapour transfer. Q. J. R. Met. Soc. 106, 85–100. https://doi.org/10.1002/qj.49710644707.

Weiss, M., Jacob, F., Duveiller, G., 2020. Remote sensing for agricultural applications: a meta-review. Remote Sens. Environ. 236, 111402 https://doi.org/10.1016/j.rse.2019.111402.

Wilczak, J.M., Oncley, S.P., Stage, S.A., 2001. Sonic anemometer tilt correction algorithms. Bound.-Layer. Meteorol. 99, 127–150. https://doi.org/10.1023/A:1018966204465.

Yang, C., Fraga, H., van Ieperen, W., Trindade, H., Santos, J.A., 2019. Effects of climate change and adaptation options on winter wheat yield under rainfed Mediterranean conditions in southern Portugal. Clim. Change 154, 159–178. https://doi.org/10.1007/s10584-019-02419-4.

Zitouna-Chebbi, R., Prévot, L., Jacob, F., Mougou, R., Voltz, M., 2012. Assessing the consistency of eddy covariance measurements under conditions of sloping topography within a hilly agricultural catchment. Agric. For. Meteorol. 164, 123–135. https://doi.org/10.1016/j.agrformet.2012.05.010.

Zitouna-Chebbi, R., Prévot, L., Jacob, F., Voltz, M., 2015. Accounting for vegetation height and wind direction to correct eddy covariance measurements of energy fluxes over hilly crop fields: measuring energy flux over hilly crops. J. Geophys. Res. Atmos. 120, 4920–4936. https://doi.org/10.1002/2014JD022999.

Zitouna-Chebbi, R., Prévot, L., Chakhar, A., Marniche-Ben Abdallah, M., Jacob, F., 2018. Observing actual evapotranspiration from flux tower Eddy covariance measurements within a hilly watershed: case study of the Kamech Site, Cap Bon Peninsula, Tunisia. Atmosphere 9, 68. https://doi.org/10.3390/atmos9020068.

Zouabi, O., 2021. Climate change and climate migration: issues and questions around an in-transition Tunisian economy. Clim. Change 164, 32. https://doi.org/10.1007/s10584-021-03006-2.